Karimi *et al.*
Journal of Materials Science: Materials Theory (2024) 8:7
https://doi.org/10.1186/s41313-024-00059-5

Journal of Materials Science: Materials Theory

RESEARCH Open Access

Serrated plastic flow in deforming complex concentrated alloys: universal signatures of dislocation avalanches

Kamran Karimi[1*], Amin Esfandiarpour[1] and Stefanos Papanikolaou[1]

*Correspondence:
kamran.karimi@ncbj.gov.pl

[1] NOMATEN Centre of Excellence, National Center for Nuclear Research, ul. A. Sołtana 7, 05-400 Świerk, Otwock, Poland

Abstract

Under plastic flow, multi-element high/medium-entropy alloys (HEAs/MEAs) commonly exhibit complex intermittent and collective dislocation dynamics owing to inherent lattice distortion and atomic-level chemical complexities. Using atomistic simulations, we report on an avalanche study of model face-centered cubic (fcc) NiCoCrFeMn and NiCoCr chemically complex alloys aiming for microstructural/topological characterization of associated dislocation avalanches. The results of our avalanche simulations reveal a close correspondence between the observed serration features in the stress response of the deforming HEA/MEA and the incurred slip patterns within the bulk crystal. We show that such correlations become quite pronounced within the rate-independent (quasi-static) regime exhibiting scale-free statistics and critical scaling features as universal signatures of dislocation avalanches.

Keywords: avalanches, high entropy alloys, crystal plasticity, dislocations, strain bursts, serrations

Introduction

The serrated response is a commonly observed phenomenon in a broad class of driven systems (Fisher 1998). Examples include crackling sounds due to plasticity (Miguel et al. 2001; Sultan et al. 2022; Karimi 2017) or brittle fracture (Vu et al. 2019; Petri et al. 1994; Karimi et al. 2019), Barkhausen noise in ferromagnetism (Durin and Zapperi 2000) and even stick-slip dynamics of earthquakes at geological scales (Scholz 2002), just to name a few. Under a sufficiently slow driving rate, serrations refer to highly-intermittent and irrecoverable dynamics that a quiescent (but driven) system undergoes, beyond its threshold, as a certain form of relaxation. As for serrated plastic flow in deforming crystalline solids (Brechtl et al. 2020), the relaxation process typically occurs through slip bursts mainly due to the spontaneous nucleation/depinning of dislocations that exhibit a collective motion within the bulk leading to the so-called dislocation avalanches. The scale-free nature of dislocation avalanches —featuring a broad range of time, length, and energy scales (Zaiser 2006)— may indeed suggest some form of criticality/universality within the context of yielding transition (Friedman et al. 2012). The notion of universality is not always strictly defined in light of close ties between avalanche statistics and

dislocations' substructure as well as their complex mechanisms of nucleation, glide, and interactions which are believed to show certain non-universal features (Richeton et al. 2005; Sparks et al. 2018), depending on various factors such as crystalline phase, lattice orientation, chemical composition, specimen size, temperature, and deformation rate sensitivity. Given the above considerations, how could we infer such complex dislocation patterns and underlying interaction mechanisms by probing statistics of dislocation avalanches? The question posed here has very practical implications in the context of nanomechanical testing methods that, together with in-situ imaging techniques, can give us rich knowledge and insights about nanoscopic origins of plasticity.

The existing literature has a wealth of experimental information on serration features of driven crystalline metals and associated microstructural signatures across a broad range of laboratory settings (see Papanikolaou et al. (2017) and references therein). This includes a large suite of nano/micro scale mechanical tests (e.g. uniform tension, nano/micro pillars, nano-indentation) that are typically supplemented by acoustic emission (AE) measurements of intermittent bursts and/or in(ex)-situ microscopy. A rather generic observation is the power-law distributed magnitude of the latter $P(S) \propto S^{-\tau}$ but with scaling exponent τ that gets typically affected by underlying mechanisms at play and shows deviations from the mean-filed estimate 3/2 (Fisher 1998). The experimental range mostly observed for pure metals (Ni, Al, Cu, Au, Mo, and Nb) is between $\tau = 1.5 - 1.9$ (Papanikolaou et al. 2017; Rizzardi et al. 2022), bearing in mind that various metrics have been proposed as avalanche size based on types of experimentation and associated observables. In-situ electron-microscopy-based investigations have been mainly centered on establishing meaningful links between the occurrence of plastic avalanches and coinciding microstructural evolution. In this context, significant size effects have been commonly identified in both stress serration features and dislocation morphologies, with the latter mainly arising from surface-induced limitations of deformation sources and augmented annhilation mechanisms (Shan et al. 2008; Oh et al. 2009; Kiener and Minor 2011; Maaß et al. 2007). Rate effects (Zhang et al. 2013) have been consistently reported to influence dislocation glide mechanisms and associated relaxation processes which were shown to systematically alter statistics of slip avalanches (Papanikolaou et al. 2012; Ananthakrishna et al. 1999).

Overall, the aforementioned studies suggest certain *indirect* (but insightful) links between serrated flow features and dislocation slip patterns in pure crystalline metals. Such correlations become even more challenging within the framework of high/medium-entropy alloys (HEAs/MEAs), bearing in mind inherent atomic-level complexities, due to underlying lattice distortions, which are known to be the dominant source of HEAs/MEAs' exceptional properties (Li et al. 2019; Shang et al. 2021). Unlike conventional alloys, these complex concentrated alloys possess a rugged energy landscape giving rise to intrinsic randomness in local Peierls stresses and, therefore, unusual pinning patterns and jerky glide dynamics of roughened dislocations (Li et al. 2019; Zhang et al. 2019). A relevant study by Hu et al. (2018) demonstrated the accumulation of dislocation bands and pile-ups in a compressed HEA nanopillar, owing to the complex interplay with random obstacles, that significantly differs from the surface-induced annhilation mechanism observed in pure fcc metals. Another complication arises from compositional/microstructural heterogeneities (local chemical ordering (Zhang et al. 2020; Wu et al. 2021), nano-precipitation (Ardell 1985), deformation-induced phase transition

(Basu and De Hosson 2020)) that interplay with dynamics of dislocations in often unpredictable and inextricable ways (Naghdi et al. 2023) in chemically complex alloys. Prior applications of AE tests, as the gold standard in the field, mainly reported certain critical features of jerky plastic flow and associated strain bursts in HEAs (Chen et al. 2022b, a; Brechtl et al. 2023) but did not fully succeed in directly associating their temporal dynamics to bulk substructural features (Ahmed et al. 2021). In-situ characterization of nanoscale deformation patterns in combination with AE experiments has been practically challenging due to complex microstructural origins of acoustic signals, highly-specialized instrumentation, and sample preparation difficulties.

Here in this study, our aim is to explore such microstructure-property correlations in the single-phase face-centered cubic (fcc) NiCoCrFeMn and NiCoCr as two exemplary HEA and MEA. We seek for potential microstructural footprints in avalanche statistics to gain further understanding into underlying atomic-level deformation mechanisms. To this end, we perform atomistic simulations of model Cantor and NiCoCr alloys under uniaxial tension and analyze serration features of the stress response together with the incurred slip patterns within the bulk sample. As a comparative study, we further investigate avalanche properties in pure Ni which lacks the chemical/microstructural heterogeneity element (owing to lattice distortion) as in Cantor and NiCoCr alloys but still features nontrivial avalanche properties. We, in particular, probe deformation rate effects on spatial-temporal evolution of slip events and their statistics at room temperature. We find that dislocation avalanches in the driven HEA and MEA exhibit a scale-free process characterized by asymptotic power-law regimes and critical scaling exponents that govern serrated plastic flow but show minimal variations with respect to the chemical composition. Our findings indicate that the morphology of microstructural changes is strongly rate-dependent and exhibits meaningful correlations with avalanche size statistics within a rate-independent regime.

The paper's layout is as follows. In Methods & protocols section, we describe the numerical setup, sample preparation, loading protocols, and relevant simulation details including interatomic forces and shear test description. Results section presents our simulation results relevant to investigations of dislocation avalanches followed by a phase analysis of the microstructure as well as their potential correlations under different deformation rates. In this context, Avalanche analysis: size & duration section examines avalanche statistics (size and duration) to characterize their rate-dependence. Microstructural signatures of dislocation avalanches will be discussed in Microstructural analysis: crystal phase, cluster statistics, and slip planes and Correlation analysis: dislocation avalanches & microstructure sections. Conclusions & discussions section presents relevant discussions and conclusions.

Methods & protocols

We performed molecular dynamics simulations in LAMMPS (Thompson et al. 2022) by implementing atomistic samples of size $N = 10,000$ within a three-dimensional periodic cell. We prepared cubic samples with dimension $L = 40$ Å along the x[100], y[010], and z[001] directions. The NPT ensembles were implemented via a Nose-Hoover thermostat and barostat with relaxation time scales $\tau_d^{\text{therm}} = 10$ fs and $\tau_d^{\text{bar}} = 100$ fs ($1\ \text{fs} = 10^{-15}$ s). We also set the discretization time to $\Delta t = 1.0$ fs. Samples were initially prepared via

an energy minimization at $T = 0$ K (at a fixed pressure) and subsequently thermalized at room temperature ($T = 300$ K) and constant pressure $P = 0$ bar for the duration of 100 ps prior to loading. The interatomic forces were derived from the modified embedded-atom method potential developed recently by Choi et al. (2018). Tensile tests were carried out by deforming the z dimension of the simulation box at constant strain rates $\dot{\epsilon}_{zz} = 10^8 - 10^{10}$ s^{-1} with $P_{xx} = P_{yy} = 0$. We remark the limitation of atomistic simulations in accessing realistic experimental timescales. Although the deformation rates in our numerical study exceed those found in experiments by orders of magnitude, our simulations effectively capture crucial rate effects, including the dynamical transition from stick-slip-like behavior to homogeneous flow once a specific rate threshold is surpassed. We performed additional simulations at deformation rates 0.5×10^8, 0.25×10^8 s^{-1} and conducted avalanche analyses, ensuring that the statistical size distributions and estimated size exponents τ remain consistent and robust within the quasi-static limit.

Results

We performed a series of tensile tests on model Cantor, NiCoCr, and Ni alloys at different deformation rates and room temperature. The evolution of the (normal) stress σ_{zz} with the tensile strain ϵ_{zz} and the associated rate $\partial_t \sigma_{zz}$ are plotted in Fig. 1a at $T = 300$ K and $\dot{\epsilon}_{zz} = 10^8$ s^{-1} corresponding to NiCoCrFeMn. Due to the defect-free crystalline lattice used in the simulation, the initial plastic deformation occurs at a significantly high stress level ($\simeq 8$ GPa), likely corresponding to the critical resolved shear stress of Ni on (111) planes (5 GPa) (Shimanek et al. 2022).

Upon yielding, the mechanical response is characterized by a stick-slip-type behavior with abrupt force drops preceded by longer stress build-up periods as in Fig. 1b. Similarly, the stress rate exhibits an intermittent dynamics with quiescent periods (i.e., $\partial_t \sigma_{zz} \simeq 0$) that are frequently interrupted by fairly short-lived bursts of events. The latter are typically accompanied by slips across close-packed {111} atomic planes in a fcc structure to form hcp layers within stacking fault regions as in Fig. 1e and f. Figure 1c and d displays the fraction of atoms with hcp(bcc) structure $\rho_{\text{hcp(bcc)}}$ and its evolution with time t. In what follows, we identify individual stress avalanches and probe their statistics (i.e., size and duration) showing non-trivial correlations with the structure of slip planes at low strain rates.

Avalanche analysis: size & duration

We define the avalanche size as the magnitude of the stress drop $S = -\int_{t_i}^{t_i+\mathcal{T}_i} \partial_t \sigma_{zz}\, dt$ corresponding to event i initiated at t_i with duration $\mathcal{T}_i$ as illustrated in Fig. 1b. During the avalanche period, the stress rate exceeds a threshold value set by the median rate, $-\partial_t \sigma_{zz} \geq \dot{\sigma}_{\text{th}}$ with $\dot{\sigma}_{\text{th}} = \text{median}(-\partial_t \sigma_{zz})$. We also checked the robustness of our results against variations in $\dot{\sigma}_{\text{th}}$ (data not shown). To remove the thermal noise from the stress signal, we use the optimal (Wiener) filtering (see the Supplementary Materials for further details) and ensure that our avalanche analysis is performed on sufficiently smooth timeseries. We systematically gather statistics of avalanches incurred at the strain interval $\epsilon_{zz} = 0.2 - 1.0$ within the steady-state flow regime. This is to ensure that we probe dynamics within the steady-state flow regime discarding transient effects due to initial yielding. We also checked that smaller strain intervals have

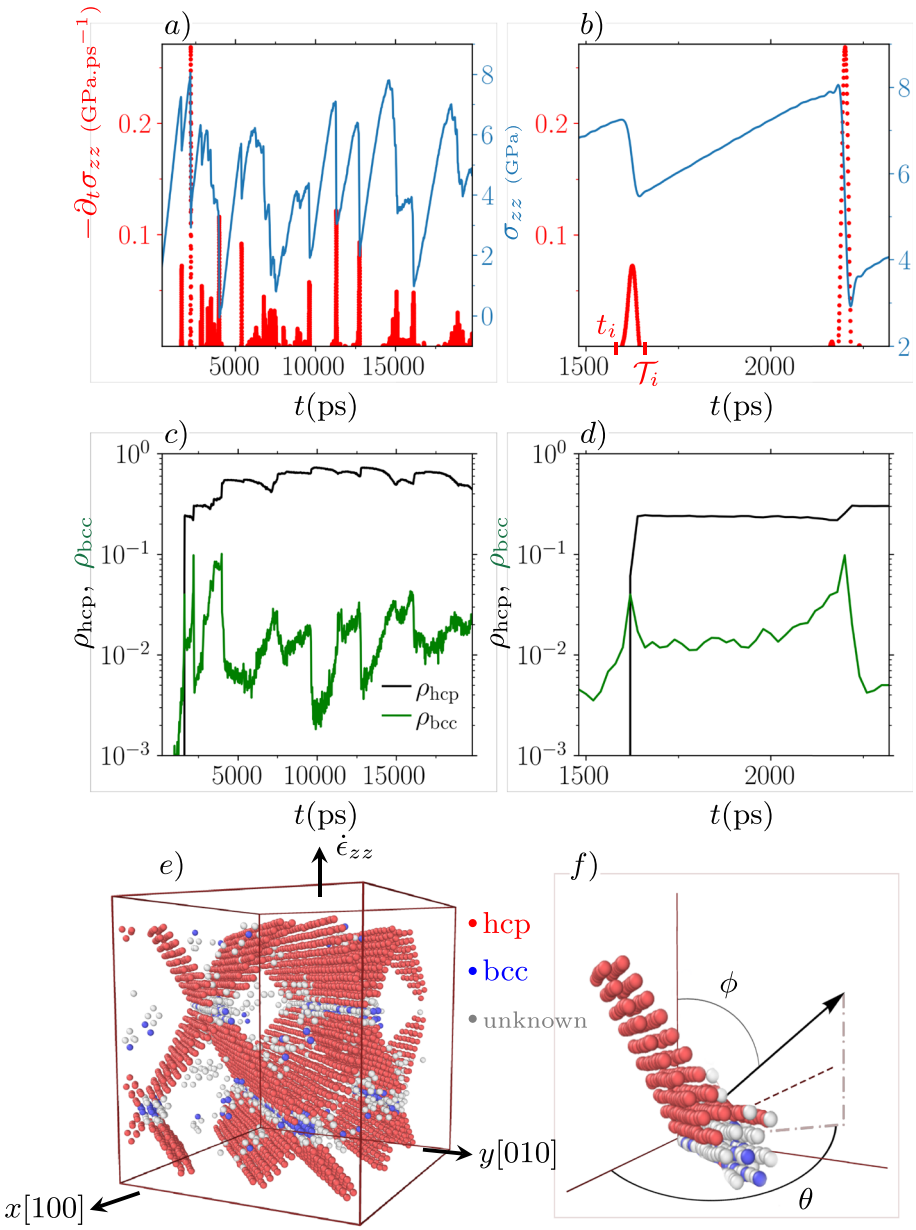

Fig. 1 **a** The evolution of the normal stress σ_{zz} and spontaneous stress rate $\partial_t \sigma_{zz}$ with time t at $T = 300$ K and $\dot{\epsilon}_{zz} = 10^8$ s^{-1} corresponding to the Cantor alloy. **b** A magnified view of (**a**) with the i-th avalanche starting at t_i and having the duration of $\mathcal{T}_i$. **c**) Fraction of atoms $\rho_{\rm hcp}$ and $\rho_{\rm bcc}$ with hcp and bcc arrangement versus time. **d** A magnified view of (**c**). **e** Illustration of the uniaxial setup with the formation of the hcp clusters of atoms within {111} slip planes during an avalanche. **f** Crystallographic orientation of a hcp cluster of size $s_{\rm hcp}$ described by the azimuthal angle θ and polar angle ϕ

very insignificant effects on statistics of dislocation avalanches and the latter is fairly robust across these variations. To improve the collected statistics, we consider fairly large statistical ensembles with order $10 - 100$ realizations per deformation rate. The avalanche analysis is performed on an extensive dataset, typically including around $10^3 - 10^4$ avalanches in each case, to ensure the robustness and accuracy of the estimated scaling exponents.

Figure 2a-f displays the scatter plot of the avalanche size S and event duration $\mathcal{T}$, scaled by $\dot{\epsilon}_{zz}^{-1}$, as well as size distributions $P(S)$ at $T = 300$ K and various rates $\dot{\epsilon}_{zz}$ corresponding to Cantor alloy, NiCoCr, and pure Ni. The scatter plots in Fig. 2a, c, and e demonstrate that, statistically speaking, larger avalanches tend to have longer duration with a scaling behavior that may be described on average as $\langle S \rangle \propto \mathcal{T}^{\gamma}$ with $\gamma \simeq 1.0$. The observed scaling regime appears to be fairly limited at the slowest rate $\dot{\epsilon}_{zz} = 10^8$ s^{-1} with the duration that tends to saturate at large avalanche sizes, possibly due to size effects. In Fig. 2b, the size distribution associated with the slowest rate in Cantor alloy decays as a power-law $P(S) \propto S^{-\tau}$ (above a certain cut-off size $S_c \simeq 10^{-1}$ GPa) which spans at least two

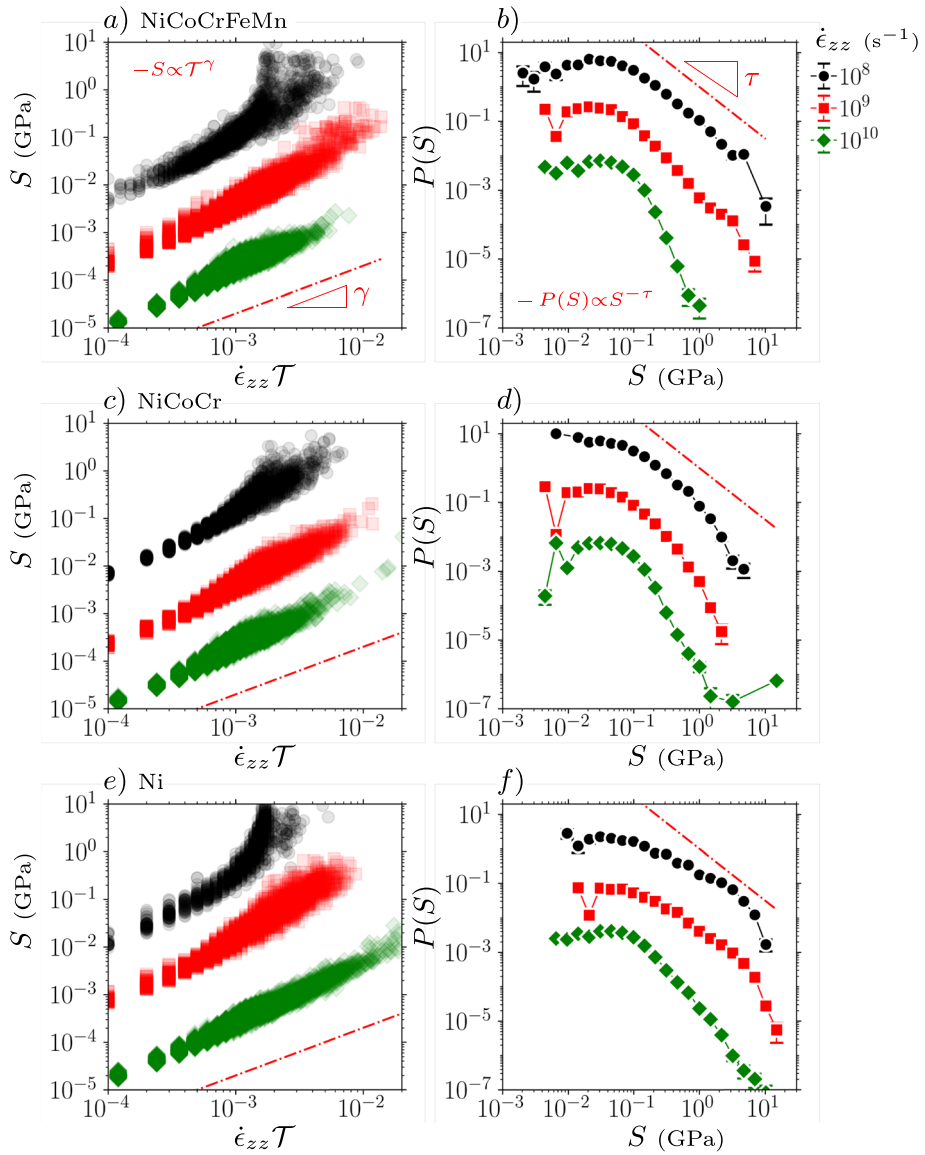

Fig. 2 Avalanche statistics at $T = 300$ K and multiple strain rates $\dot{\epsilon}_{zz}$ corresponding to NiCoCrFeMn, NiCoCr, and Ni. **a**, **c**, **d** Scatter plot of avalanche size S and scaled duration $\dot{\epsilon}_{zz}\mathcal{T}$ **b**, **d**, **f** avalanche size distributions $P(S)$. The dashdotted lines denote power laws **a**, **c**, **e** $S \propto \mathcal{T}^{\gamma}$ with $\gamma = 1.0$ **b, d, f**) $P(S) \propto S^{-\tau}$ with $\tau = 3/2$. The error bars indicate standard errors. The data are shifted vertically for the sake of clarity. , maintaining the underlying scaling behavior on the log-log scale

decades in S and seems to be well-predicted by the mean-field estimate $\tau = 3/2$ (Fisher 1998). As $\dot{\epsilon}_{zz}$ is increased toward 10^{10} s^{-1}, the size distributions tend to exhibit a steeper fall-off with a nearly exponential-like drop at the fastest deformation rate. We observe very similar trends for avalanche statistics in NiCoCr as in Fig. 2c and d in terms of the rate dependence, except for a comparatively limited power-law scaling regime associated with $P(S)$ at $\dot{\epsilon}_{zz} = 10^8$ s^{-1}. The scaling between the size and duration in the case of pure Ni closely resembles that of the two alloys as in Fig. 2e. However, the avalanche size exponent in Fig. 2f is notably shallower than the mean-field prediction $\tau < 3/2$ at the slowest rate but tends to become more mean-field like at the intermediate strain rate. We note that the observed power-law behavior in Ni appears to be quite sensitive to the filtering process and slight variations in the relevant parameters lead to a better agreement with theoretical predictions (refer to Fig. S3c).

Microstructural analysis: crystal phase, cluster statistics, and slip planes

We aim to probe the relevance of the classical percolation theory including investigations of cluster statistics and their dynamical evolution. Additionally, we seek for potential microstructural footprints in avalanche statistics including investigations of crystal phases and their correlations with plastic avalanches. As a structural metric associated with dislocation avalanches, we identified atomic structure types via the common neighbor analysis implemented in OVITO (Stukowski 2009), seeking for atoms in hexagonal close-packed (hcp) and body-centered cubic (bcc) arrangements. The hcp atoms are associated with stacking faults which are bounded by partial dislocations in a face-centered cubic (fcc) structure.

We investigated statistics of hcp clusters (including size and orientation) and sought for their correlations with stress avalanches. Here a cluster is defined as a set of adjacent atoms with the same structural type —hcp in this study. As a basic statistical property, $P(s_{\text{hcp}})$ denotes the probability distribution function associated with the number of clusters containing s_{hcp} atoms. The radius of gyration associated with a cluster of size s_{hcp} may be also defined as $r_g = \sum_{i=1}^{s_{\text{hcp}}} |\mathbf{r}_i - \mathbf{r}_0|^2 / s_{\text{hcp}}$ with the center of mass $\mathbf{r}_0 = \sum_{i=1}^{s_{\text{hcp}}} \mathbf{r_i} / s_{\text{hcp}}$. Figure 3a, c, and e illustrates that $s_{\text{hcp}} \propto r_g^{d_f}$ with fractal dimension $d_f \simeq 2.0$. This almost agrees with Fig. 1e and f in the sense that, on average, hcp-type clusters tend to form fairly planar structures. At the slowest rate $\dot{\epsilon}_{zz} = 10^8$ s^{-1}, the proposed scaling seems to be quite consistent with observations for NiCoCr and Ni in Fig. 3c and e whereas Cantor alloy in Fig. 3a exhibits a slightly larger scatter in measurements likely due to microstructural heterogeneities.

Figure 3b, d, and f plots $P(s_{\text{hcp}})$ at different strain rates. We note that the cluster size distributions develop fairly long tails with decreasing $\dot{\epsilon}_{zz}$, due to system-spanning slip planes, with a decay that can be best described by a power-law $P(s_{\text{hcp}}) \propto s_{\text{hcp}}^{-\tau_c}$ over at least two decades in s_{hcp}. Here the distributions show a meaningful rate-dependence with the trend already observed for avalanche size distributions in Fig. 2b and d. Nevertheless, we see a slower-than-predicted decay of $P(s_{\text{hcp}})$ at the slowest rate —$\tau_c < \tau_{\text{pred}} = 2$ as inferred from percolation theory (Stauffer and Aharony 2018)— for the three metals which crossovers to the predicted (mean-field) behavior at faster deformation rates.

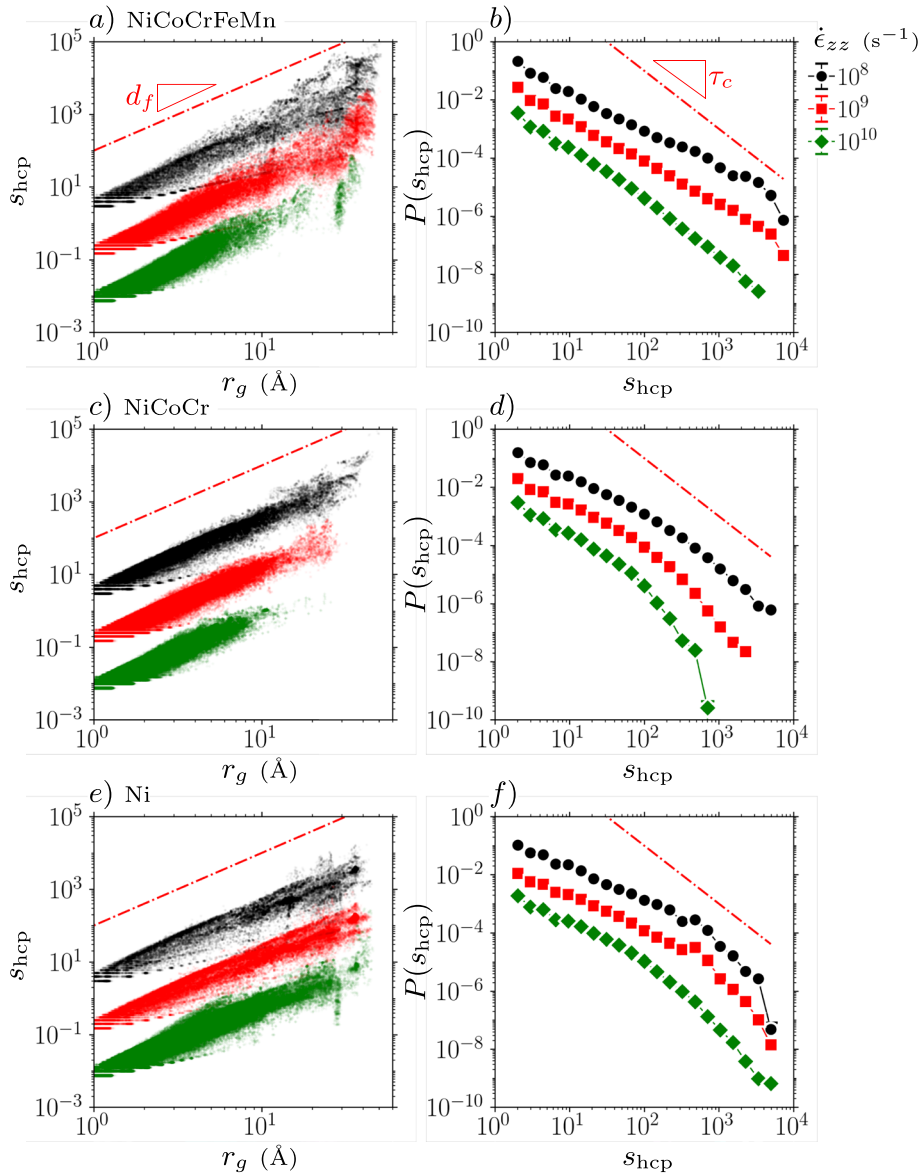

Fig. 3 Cluster size statistics at different strain rates $\dot{\epsilon}_{zz}$ associated with NiCoCrFeMn, NiCoCr, and Ni. **a**, **c**, **e** Scatter plot of cluster size s_{hcp} and associated radius of gyration r_g **b**, **d**, **f** Cluster size distribution $P(s_{\mathrm{hcp}})$. The dashdotted lines denote power laws **a**, **c**, **e** $s_{\mathrm{hcp}} \propto r_g^{d_f}$ with $d_f = 2$ **b**, **d**, **f** $P(s_{\mathrm{hcp}}) \propto s_{\mathrm{hcp}}^{-\tau_c}$ with $\tau_c = 2$. The error bars indicate standard errors. The data are shifted vertically for the sake of clarity

Having analyzed the size distributions of hcp clusters, we now turn to their crystallographic orientation relationship. The latter is described based on the azimuthal angle θ and polar angle ϕ measured from the lattice coordinate frame as in Fig. 1f. The density plots presented in Fig. 4 correspond to orientation maps (θ, ϕ) at three different strain rates. Within these maps, the black (solid) circles denote the {111} and {100} orientations corresponding to the undeformed crystals as in Fig. 1e.

Our data in Fig. 4a confirm that, statistically speaking, hcp glide planes tend to align with four different sets of {111} closed-packed planes in Cantor alloy. The density maps also suggest a fair amount of activation in the vicinity of the {100} family

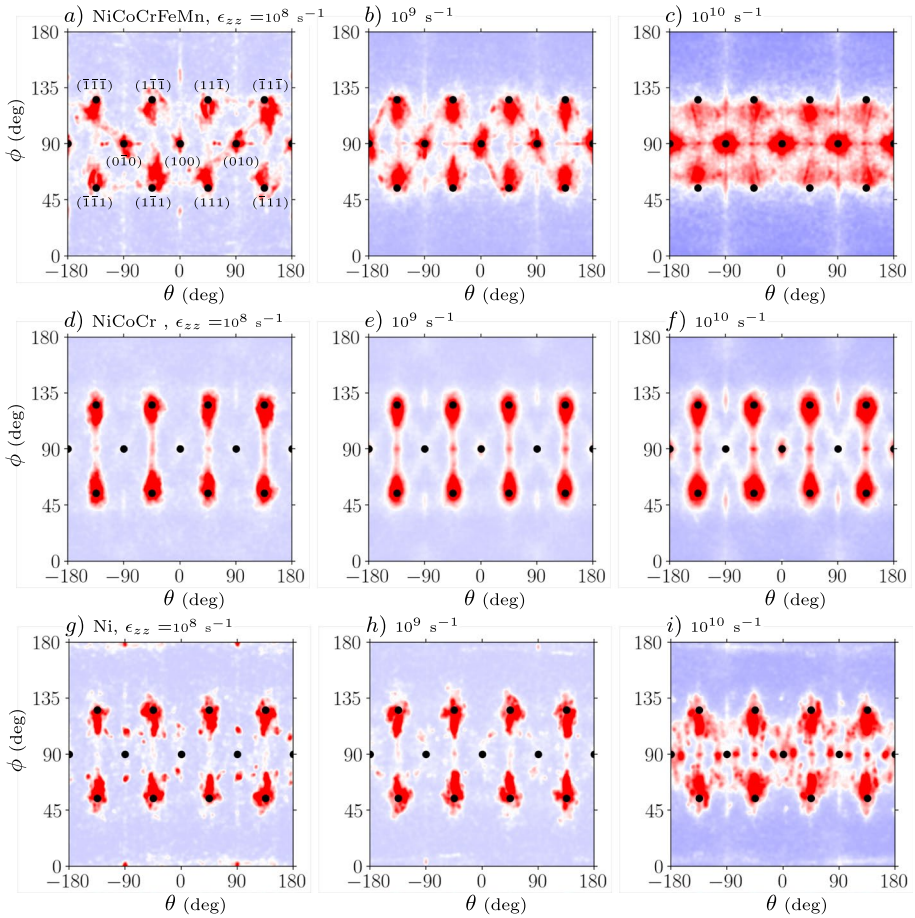

Fig. 4 Orientation density maps (θ, ϕ) associated with hcp glide planes at various deformation rates $\dot{\epsilon}_{zz}$ corresponding to **a**-**c** Cantor alloy, **d**-**f** NiCoCr, and **g**-**i** pure Ni. The (black) symbols denote different crystallographic planes as in Fig. 1. The red and blue colors denote high and low densities, respectively

which are mostly due to the loading-induced *reorientation* of the slip planes. We note that uniaxial tension is performed normal to the (001) plane with $\phi = 0°, 180°$. Our assumption is that reorientation within plastic flow will not affect statistics of avalanches since plasticity initiates and continues on predicted (111) slip planes. Due to shear-induced reorientation, however, not all the four slip planes remain active during uniaxial tension.

There exists a certain amount of data scatter possibly attributed to clusters being of very small size $s_{\text{hcp}} \ll 10$ and/or numerical artifacts because of non-planar topology of hcp clusters. An increase of the deformation rate in Fig. 4b and c tends to reorient hcp planes to a larger extent as illustrated by the broader and/or denser distributions around {100}. As for NiCoCr in Fig. 4d, a relatively insignificant reorientation of slip planes appears to be relevant at the slowest rate but intensifies with increasing rates in Fig. 4e and f. Another observation is the preferential reorientation around {110} family planes (i.e. $\phi = 90°$ and $\theta = \pm 45°, \pm 135°$). In the case of pure Ni in Fig. 4g, h, and i, the metal appears to indicate fairly consistent features with Cantor alloy but with a slightly weaker reorientation of slip planes.

Correlation analysis: dislocation avalanches & microstructure

We carried out a correlation analysis between avalanche sizes S and associated changes in the fraction of hcp atoms ρ_{hcp} incurred over the duration of individual avalanches (refer to Fig. 1c and d). The latter is defined as $\Delta\rho_{\text{hcp}} = \int_{t_i}^{t_i+\mathcal{T}_i} |\partial_t \rho_{\text{hcp}}|\, dt$ corresponding to the i_{th} avalanche at t_i with duration $\mathcal{T}_i$. We also obtained the (linear) correlation coefficient $c_{XY} = \langle \hat{X}\hat{Y} \rangle$ between the two observables $X = \log_{10} S$ and $Y = \log_{10} \rho_{\text{hcp}}$. Here $\hat{X}$ indicates the deviation from the mean $\langle X \rangle$, normalized by the standard deviation std(X) associated with each variable. The above analysis was repeated for the bcc arrangement with the results shown as the scatter plots of Fig. 5 at multiple $\dot{\epsilon}_{zz}$.

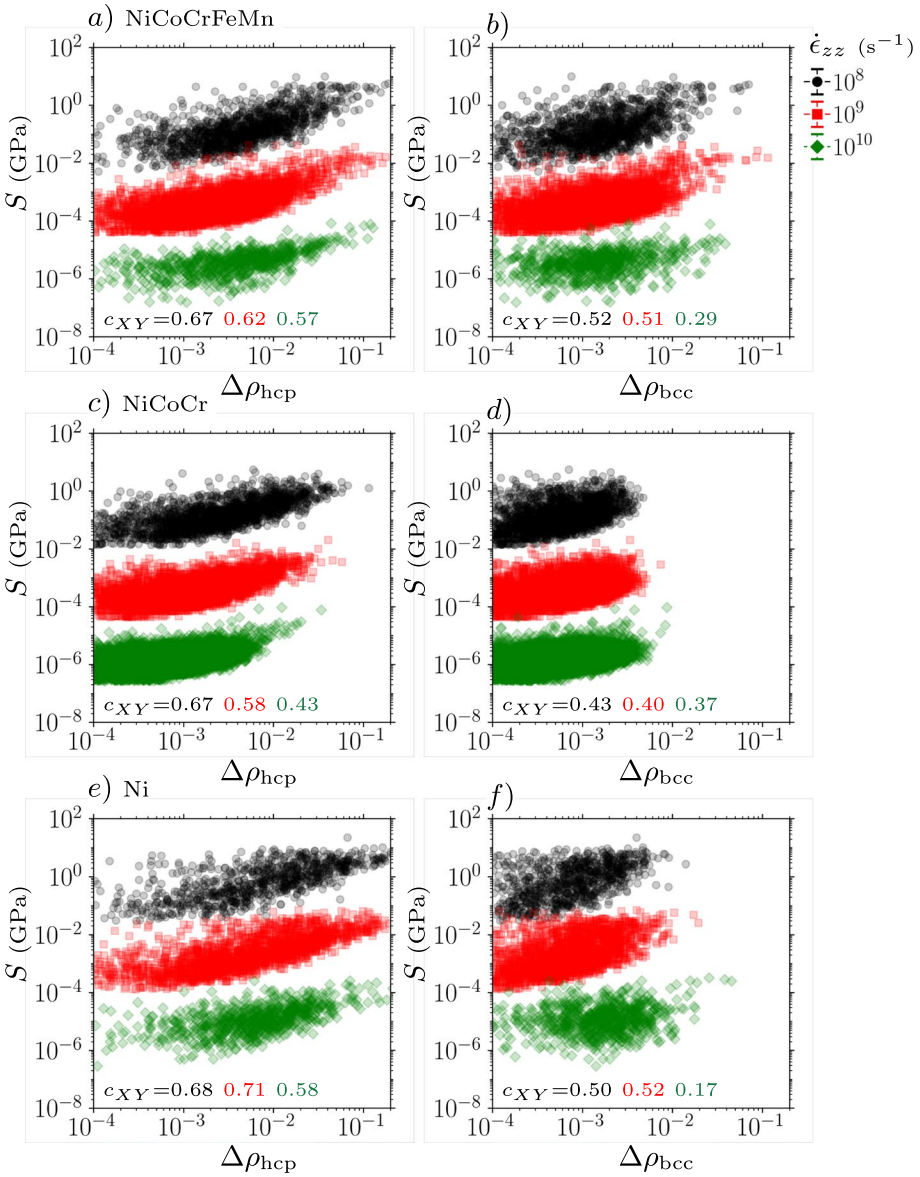

Fig. 5 Correlations between avalanche size and associated change in crystal structures corresponding to NiCoCrFeMn, NiCoCr, and pure Ni. Scatter plot of avalanche size S and the creation/annihilation ratio of **a**, **c**, **e** hcp structure $\Delta\rho_{\text{hcp}}$ **b**, **d**, **f** bcc structure $\Delta\rho_{\text{bcc}}$ at various rates $\dot{\epsilon}_{zz}$. Here c_{XY} denotes the corresponding correlation coefficient between $\Delta\rho_{\text{hcp}}$ and $\Delta\rho_{\text{bcc}}$ with S. The data are shifted vertically for the sake of clarity

Our data in Fig. 5a and b exhibit a large scatter in Cantor alloy but the observed trend indicates meaningful variations between the two sets of observables at the slowest driving rate $\dot{\epsilon}_{zz} = 10^8\ \mathrm{s}^{-1}$. Here, (positive) correlations between S and $\Delta\rho_{\mathrm{hcp}}$ (or $\Delta\rho_{\mathrm{bcc}}$) imply that avalanches of large size typically correspond to considerable microstructural changes, most likely associated with fcc-to-hcp and fcc-to-bcc phase transformations. $\Delta\rho_{\mathrm{hcp}}$ features a relatively stronger association with S, as demonstrated by larger correlation coefficients c_{XY}, suggesting that plastic avalanches are presumably rooted in partial slips and formation of layers of hcp stacking in fcc NiCoCrFeMn. With increasing $\dot{\epsilon}_{zz}$ toward $\dot{\epsilon}_{zz} = 10^{10}\ \mathrm{s}^{-1}$, such correlations become less pronounced, in particular, between avalanche sizes S and $\Delta\rho_{\mathrm{bcc}}$. Our correlation analysis associated with NiCoCr and Ni as in Fig. 5c-f reveal similar correlation patterns compared with Cantor alloy. We note that fcc-to-hcp and fcc-to-bcc phase transformations appear to have no distinguishable signatures in avalanche statistics (i.e. bimodality and/or variations in power-law exponents), or at least our methodology failed to distinguish between the two phenomena.

Conclusions & discussions

Our atomistic simulations have clearly indicated the close relevance of the scale-free nature of dislocation avalanches in HEAs. This scale-invariance has been evidenced by robust scaling features (under "quasi-static" drive) described by asymptotic power-law distributions and associated critical exponents that, in general, match empirical evaluations as well as mean-field predictions. More specifically, the avalanche size exponents we measure are fairly compatible with mean-field estimates ($\tau = \frac{3}{2}$ (Fisher 1998; Friedman et al. 2012; Antonaglia et al. 2014)) and within the experimentally reported range $1.3 - 2.0$ (Chen et al. 2022b; Antonaglia et al. 2014; Rizzardi et al. 2021) in chemically complex alloys. Notably, NiCoCr exhibits a fairly restricted scaling regime associated with avalanche size distributions that is possibly attributed to strong heterogeneities and large atomic misfits (Esfandiarpour et al. 2022), driving this alloy away from criticality. One should also take the above estimates with grain of salt as various metrics have been utilized as avalanche size in the literature including (but not limited to) slip magnitude, stress drop, and emitted (acoustic) energies. The observed rate effects on statistics of dislocation avalanches are in line with experimentation on HEAs/MEAs that indicate dynamical cross-overs between different serration types at a certain range of deformation rates (see Brechtl et al. (2020) and references therein). Beyond a certain rate threshold, the three deforming metals undergo a dynamical transition into a subcritical state characterized by non-critical exponential-like statistics of avalanches. We further speculate that the elevation/reduction of testing temperature, while maintaining the same quasi-static driving rate, may also lead to a transition of serration modes as reported by Wei et al. (2023).

To discern the role of local lattice distortions associated with the Cantor and NiCoCr alloys, we have additionally probed statistics of avalanches in pure Ni showing fairly consistent features with the former metals in terms of the overall rate dependency. Nevertheless, we have found a relatively shallow decay of avalanche size distributions within the quasi-static regime exhibiting a non-mean-field behavior $\tau < \frac{3}{2}$ which was also reported in two-dimensional dislocation dynamics simulations (Ispánovity et al. 2014). This might be indicative of the relative abundance of big avalanches over small ones in

the pure metal possibly due to the absence of chemical/structural disorder. In certain alloys, this heterogeneity element may act as effective obstacles against propagating avalanches and, therefore, strongly influence their statistical properties, often resulting in the dominance of smaller-size avalanches. We conjecture that the disorder strength and associated length might be relevant parameters that govern the critical exponent τ and its deviation from the mean-field prediction.

On the origin of the different statistical behavior observed in HEA/MEA compared to Ni, one might hypothesize that the former alloys would relatively favor the shear of {111} planes, given the known negative stacking fault energy γ_{sf} of NiCoCr and NiCoCrFeMn at 0 K (Zhao et al. 2017; Baruffi et al. 2023). We argue that, theoretically speaking, γ_{sf} should not control the decay behavior associated with avalanche size statistics (i.e. τ) which, instead, only depends on the two independent exponents d_f and τ_c. The observed discrepancy in size distributions cannot be solely ascribed to variations in the fault energies but appears to originate from lattice distortions and solute hardening effects as relevant mechanisms that tend to curtail slip events. This hypothesis could be potentially tested in future numerical and/or experimental studies.

Our microstructural analyses have demonstrated nontrivial scaling features associated with the dynamics and topology of slip planes that could be better understood in the context of percolation transition. In this framework, we find robust power-law distributed cluster sizes with scaling exponent $\tau_c \simeq 1.0$ at a rate-independent regime that is shallower than the mean-field prediction $\tau_c^{\text{mf}} = 2$ (Stauffer and Aharony 2018) in the studied metals but cross-overs to the latter exponent at intermediate rates beyond which the cluster size distribution enters a subcritical regime, analogous to avalanche size distributions. We note that Ni features a non-mean-field scaling for both avalanche size S and cluster size s_{hcp} distributions in the rate-independent regime. As for Cantor alloy (and to some degree NiCoCr alloy), the former distribution indicates an asymptotic mean-field behavior. This is rather counter-intuitive as one would naively expect the two observables to intercorrelate strongly. Our speculation is that, due to underlying disorder in the HEA (and/or MEA), plastic avalanches may primarily occur as a result of the accumulation of broadly-distributed yet *randomly*-triggered individual slips. By contrast, the observed trends associated with pure Ni might be indicative of spatial and/or temporal correlations between the latter. Our correlation analysis may establish a direct mapping between avalanches of certain size and incurred slip patterns within a rate-independent regime. Such a close correspondence between the two variables is not maintained at finite deformation rates which could be taken as another indication that high strain rates and/or stresses tend to drive these systems away from criticality.

On a separate note, our simulations do not capture surface effects as well as pre-existing defect structures as realistic phenomena in experimental scenarios. This latter feature can be understood within the broader framework of processing-microstructure-property relationships in complex alloys. In a recent micro-compression study conducted by Ugi et al. (2023), the emergence of dislocation loops in irradiated Zn resulted in an initial hardening response, accompanied by the suppression of plastic bursts. Notable surface effects, predominant in small-scale experiments, were systematically observed, primarily attributed to limitations on deformation sources and heightened annihilation mechanisms (see Introduction section and associated references). With that

said, our simple numerical setup is still able to capture certain (if not all) empirical features of serrated plastic flow (i.e. scale-free statistics) but within limits. In fact, a one-to-one comparison between the simulated stress release mechanisms and laboratory-based observations requires implementing further details (i.e. free surface and pre-existing defects) to ensure the accuracy and validity of the conclusions drawn.

Our findings on the strong coupling between temporal and spatial evolution of dislocation avalanches may contribute to ongoing efforts within the material science and physics communities that aim to infer underlying morphology and microstructural changes by solely probing the mechanical signals. Recently, the state-of-the-art machine learning models have emerged as robust computational tools to classify/reconstruct the bulk micro-structure based on feature extraction of surface measurements (e.g. frequency content, magnitudes, signal duration, and energy scales). Combined with in-situ imaging techniques, such surrogate models and their predictions can provide a valuable insight into the microstructural origins of plasticity in a timely, efficient, and accurate manner.

Supplementary Information

The online version contains supplementary material available at https://doi.org/10.1186/s41313-024-00059-5.

Supplementary Material 1.

Acknowledgements
We wish to acknowledge insightfull discussions with M. Alava. This research was funded by the European Union Horizon 2020 research and innovation program under grant agreement no. 857470 and from the European Regional Development Fund via Foundation for Polish Science International Research Agenda PLUS program grant no. MAB PLUS/2018/8. The publication was created within the framework of the project of the Minister of Science and Higher Education "Support for the activities of Centres of Excellence established in Poland under Horizon 2020" under contract no. MEiN/2023/DIR/3795.

Authors' contributions
AE performed avalanche simulations relevant to slowly-deforming complex concentrated alloys. KK carried out the avalanche analysis and was a major contributor in writing the manuscript. SP initiated and supervised the current study and made a significant contribution by reviewing and editing the manuscript. All authors read and approved the final manuscript.

Declarations

Competing interests
The authors declare no competing interests.

Received: 7 October 2023 Accepted: 19 March 2024
Published online: 11 April 2024

References

J. Ahmed, T. Zhang, D. Ozevin, M. Daly, A multiscale indentation-based technique to correlate acoustic emission with deformation mechanisms in complex alloys. Mater. Charact. **182**, 111575 (2021)
G. Ananthakrishna, S. Noronha, C. Fressengeas, L. Kubin, Crossover from chaotic to self-organized critical dynamics in jerky flow of single crystals. Phys. Rev. E **60**(5), 5455 (1999)
J. Antonaglia, X. Xie, Z. Tang, C.W. Tsai, J. Qiao, Y. Zhang, M. Laktionova, E. Tabachnikova, J. Yeh, O. Senkov et al., Temperature effects on deformation and serration behavior of high-entropy alloys (heas). Jom **66**, 2002–2008 (2014)
A.J. Ardell, Precipitation hardening. Metall. Trans. A **16**, 2131–2165 (1985)
C. Baruffi, M. Ghazisaeidi, D. Rodney, W. Curtin, Equilibrium versus non-equilibrium stacking fault widths in nicocr. Scripta Mater. **235**, 115536 (2023)
I. Basu, J.T.M. De Hosson, Strengthening mechanisms in high entropy alloys: fundamental issues. Scr. Mater. **187**, 148–156 (2020)
J. Brechtl, S. Chen, C. Lee, Y. Shi, R. Feng, X. Xie, D. Hamblin, A.M. Coleman, B. Straka, H. Shortt et al., A review of the serrated-flow phenomenon and its role in the deformation behavior of high-entropy alloys. Metals **10**(8), 1101 (2020)

J. Brechtl, R. Feng, P.K. Liaw, B. Beausir, H. Jaber, T. Lebedkina, M. Lebyodkin, Mesoscopic-scale complexity in macroscopically-uniform plastic flow of an al0. 3cocrfeni high-entropy alloy. Acta Mater. **242**, 118445 (2023)
Y. Chen, B. Gou, B. Yuan, X. Ding, J. Sun, E.K. Salje, Multiple avalanche processes in acoustic emission spectroscopy: Multibranching of the energy-amplitude scaling. Phys. Status Solidi (b) **259**(3), 2100465 (2022a)
Y. Chen, K. Tang, B. Gou, F. Jiang, X. Ding, E.K. Salje, Acoustic emission spectra and statistics of dislocation movements in fe40mn40co10cr10 high entropy alloys. J. Appl. Phys. **132**(8), 080901 (2022b)
W.M. Choi, Y.H. Jo, S.S. Sohn, S. Lee, B.J. Lee, Understanding the physical metallurgy of the cocrfemnni high-entropy alloy: an atomistic simulation study. npj Comput. Mater. **4**(1), 1–9 (2018)
G. Durin, S. Zapperi, Scaling exponents for barkhausen avalanches in polycrystalline and amorphous ferromagnets. Phys. Rev. Lett. **84**(20), 4705 (2000)
A. Esfandiarpour, S. Papanikolaou, M. Alava, Edge dislocations in multicomponent solid solution alloys: Beyond traditional elastic depinning. Phys. Rev. Res. **4**(2), L022043 (2022)
D.S. Fisher, Collective transport in random media: from superconductors to earthquakes. Phys. Rep. **301**(1–3), 113–150 (1998)
N. Friedman, A.T. Jennings, G. Tsekenis, J.Y. Kim, M. Tao, J.T. Uhl, J.R. Greer, K.A. Dahmen, Statistics of dislocation slip avalanches in nanosized single crystals show tuned critical behavior predicted by a simple mean field model. Phys. Rev. Lett. **109**(9), 095507 (2012)
Y. Hu, L. Shu, Q. Yang, W. Guo, P.K. Liaw, K.A. Dahmen, J.M. Zuo, Dislocation avalanche mechanism in slowly compressed high entropy alloy nanopillars. Commun. Phys. **1**(1), 61 (2018)
P.D. Ispánovity, L. Laurson, M. Zaiser, I. Groma, S. Zapperi, M.J. Alava, Avalanches in 2d dislocation systems: Plastic yielding is not depinning. Phys. Rev. Lett. **112**(23), 235501 (2014)
K. Karimi, D. Amitrano, J. Weiss, From plastic flow to brittle fracture: Role of microscopic friction in amorphous solids. Phys. Rev. E **100**(1), 012908 (2019)
K. Karimi, E.E. Ferrero, J.L. Barrat, Inertia and universality of avalanche statistics: The case of slowly deformed amorphous solids. Phys. Rev. E **95**(1), 013003 (2017)
D. Kiener, A.M. Minor, Source-controlled yield and hardening of cu (1 0 0) studied by in situ transmission electron microscopy. Acta Mater. **59**(4), 1328–1337 (2011)
Q.J. Li, H. Sheng, E. Ma, Strengthening in multi-principal element alloys with local-chemical-order roughened dislocation pathways. Nat. Commun. **10**(1), 3563 (2019)
Z. Li, S. Zhao, R.O. Ritchie, M.A. Meyers, Mechanical properties of high-entropy alloys with emphasis on face-centered cubic alloys. Prog. Mater. Sci. **102**, 296–345 (2019)
R. Maaß, S. Van Petegem, H. Van Swygenhoven, P.M. Derlet, C.A. Volkert, D. Grolimund, Time-resolved laue diffraction of deforming micropillars. Phys. Rev. Lett. **99**(14), 145505 (2007)
M.C. Miguel, A. Vespignani, S. Zapperi, J. Weiss, J.R. Grasso, Intermittent dislocation flow in viscoplastic deformation. Nature **410**(6829), 667–671 (2001)
A.H. Naghdi, K. Karimi, A.E. Poisvert, A. Esfandiarpour, R. Alvarez, P. Sobkowicz, M. Alava, S. Papanikolaou, Dislocation plasticity in equiatomic nicocr alloys: Effect of short-range order. Phys. Rev. B **107**(9), 094109 (2023)
S.H. Oh, M. Legros, D. Kiener, G. Dehm, In situ observation of dislocation nucleation and escape in a submicrometre aluminium single crystal. Nat. Mater. **8**(2), 95–100 (2009)
S. Papanikolaou, Y. Cui, N. Ghoniem, Avalanches and plastic flow in crystal plasticity: an overview. Model. Simul. Mater. Sci. Eng. **26**(1), 013001 (2017)
S. Papanikolaou, D.M. Dimiduk, W. Choi, J.P. Sethna, M.D. Uchic, C.F. Woodward, S. Zapperi, Quasi-periodic events in crystal plasticity and the self-organized avalanche oscillator. Nature **490**(7421), 517–521 (2012)
A. Petri, G. Paparo, A. Vespignani, A. Alippi, M. Costantini, Experimental evidence for critical dynamics in microfracturing processes. Phys. Rev. Lett. **73**(25), 3423 (1994)
T. Richeton, J. Weiss, F. Louchet, Breakdown of avalanche critical behaviour in polycrystalline plasticity. Nat. Mater. **4**(6), 465–469 (2005)
Q. Rizzardi, P. Derlet, R. Maaß, Microstructural signatures of dislocation avalanches in a high-entropy alloy. Phys. Rev. Mater. **5**(4), 043604 (2021)
Q. Rizzardi, C. McElfresh, G. Sparks, D. Stauffer, J. Marian, R. Maaß, Mild-to-wild plastic transition is governed by athermal screw dislocation slip in bcc nb. Nat. Commun. **13**(1), 1010 (2022)
C.H. Scholz, *The mechanics of earthquakes and faulting* (University Press, Cambridge, 2002)
Z. Shan, R.K. Mishra, S. Syed Asif, O.L. Warren, A.M. Minor, Mechanical annealing and source-limited deformation in submicrometre-diameter ni crystals. Nat. Mater. **7**(2), 115–119 (2008)
Y. Shang, J. Brechtl, C. Psitidda, P.K. Liaw, *Mechanical behavior of high-entropy alloys*, A review. High-Entropy Materials. Theory, Experiments, and Applications, 435-522 (2021)
J.D. Shimanek, S.L. Shang, A.M. Beese, Z.K. Liu, Insight into ideal shear strength of ni-based dilute alloys using first-principles calculations and correlational analysis. Comput. Mater. Sci. **212**, 111564 (2022)
G. Sparks, R. Maass, Shapes and velocity relaxation of dislocation avalanches in au and nb microcrystals. Acta Mater. **152**, 86–95 (2018)
D. Stauffer, A. Aharony, *Introduction to percolation theory* (Milton Park, 4 Park Square, Abingdon OX14 4RN, 2018)
A. Stukowski, Visualization and analysis of atomistic simulation data with ovito-the open visualization tool. Model. Simul. Mater. Sci. Eng. **18**(1), 015012 (2009)
N.H. Sultan, K. Karimi, J. Davidsen, Sheared granular matter and the empirical relations of seismicity. Phys. Rev. E **105**(2), 024901 (2022)
A.P. Thompson, H.M. Aktulga, R. Berger, D.S. Bolintineanu, W.M. Brown, P.S. Crozier, P.J. in 't Veld, A. Kohlmeyer, S.G. Moore, T.D. Nguyen, R. Shan, M.J. Stevens, J. Tranchida, C. Trott, S.J. Plimpton, LAMMPS - a flexible simulation tool for particle-based materials modeling at the atomic, meso, and continuum scales. Comp. Phys. Comm. **271**, 108171 (2022)
D. Ugi, G. Péterffy, S. Lipcsei, Z. Fogarassy, E. Szilágyi, I. Groma, P.D. Ispánovity, Irradiation-induced strain localization and strain burst suppression investigated by microcompression and concurrent acoustic emission experiments. Mater. Charact. **199**, 112780 (2023)

C.C. Vu, D. Amitrano, O. Plé, J. Weiss, Compressive failure as a critical transition: Experimental evidence and mapping onto the universality class of depinning. Phys. Rev. Lett. **122**(1), 015502 (2019)
S. Wei, D.P. Moriarty, M. Xu, J.M. LeBeau, On the plastic deformation of a cocrfeniw-c alloy at elevated temperatures: Part i. serrated plastic flow and its latent dynamics. Acta Mater. **242**, 118430 (2023)
Y. Wu, F. Zhang, X. Yuan, H. Huang, X. Wen, Y. Wang, M. Zhang, H. Wu, X. Liu, H. Wang et al., Short-range ordering and its effects on mechanical properties of high-entropy alloys. J. Mater. Sci. Technol. **62**, 214–220 (2021)
M. Zaiser, Scale invariance in plastic flow of crystalline solids. Adv. Phys. **55**(1–2), 185–245 (2006)
J. Zhang, G. Liu, J. Sun, Strain rate effects on the mechanical response in multi-and single-crystalline cu micropillars: Grain boundary effects. Int. J. Plast. **50**, 1–17 (2013)
L. Zhang, Y. Xiang, J. Han, D.J. Srolovitz, The effect of randomness on the strength of high-entropy alloys. Acta Mater. **166**, 424–434 (2019)
R. Zhang, S. Zhao, J. Ding, Y. Chong, T. Jia, C. Ophus, M. Asta, R.O. Ritchie, A.M. Minor, Short-range order and its impact on the CrCoNi medium-entropy alloy. Nature **581**(7808), 283–287 (2020)
S. Zhao, G.M. Stocks, Y. Zhang, Stacking fault energies of face-centered cubic concentrated solid solution alloys. Acta Mater. **134**, 334–345 (2017)

Publisher's Note